A Video-Based Support System for Nighttime Navigation in Semi-Structured Environments

Luiz Cláudio G. Andrade, Mário F. Montenegro Campos, Rodrigo L. Carceroni
Departamento de Ciência da Computação - Universidade Federal de Minas Gerais
Av. Antônio Carlos, 6627, Belo Horizonte, MG, Brazil
{lcga,mario,carceron}@dcc.ufmg.br

Abstract

This paper describes the development of a vision-based, nighttime navigation support system for automotive vehicles driving in semi-structured environments. The focus is on automatic reduction of glare produced by high beams from incoming vehicles and on generation of virtual lanes that are overlaid on the image where actual road markings should exist. To accomplish these goals, we develop video-based robust techniques that produce enhanced road images in real-time. The proposed techniques are validated by experiments with real video streams, which demonstrates the system's performance and accuracy under real conditions.

1. Introduction

This paper describes the development of a system that takes as input video streams acquired from automotive vehicles travelling at nighttime on poorly-kept roads, and outputs enhanced and augmented video streams that help human drivers navigate in those environments. More specifically, the problem solved here can be stated as: "given a stream of images of a road where traffic signs and road-marks are not reliable (or even inexistent), acquired under poor illumination conditions from a vehicle traveling at legal driving speeds, output in real-time a stream of images of the same road, in which distracting elements such as light beams from other vehicles are attenuated and consistent virtual road-marks are correctly overlaid on the images".

Night driving is riskier than day driving because of the performance reduction that the human visual system suffers at night. Detailed studies on the impact of various factors on road security found that human error is the main factor in 50% of all accidents and is a relevant factor in another 40% of them [9]. Moreover, it has been reported that fatal accidents occurring at night outnumber those occurring during the day by a factor of three to four [16]. These are the statistics in countries where roads are well maintained and properly marked. In countries with poorly-kept roads such as Brazil, night driving is even riskier.

The main motivation behind this work is to understand the central problems of nighttime driving and to minimize their impact on accidents that have human fault as their main cause, through an image enhancement system that assists drivers in less-than-favorable conditions such as those typically found in Brazilian roads.

Road and lane detection is a subject extensively researched in the field of *Intelligent Transportation Systems* (ITS). However, most approaches reported so far [10, 3] are strongly context- and application-dependent. At least two fundamental assumptions are shared by such approaches: (1) that roads are well structured, *i.e.*, they are adequately marked and traffic signs not only exist where needed, but are adequately maintained and clearly visible; and (2) that image acquisition is performed at daytime. The first assumption makes the detection of important visual features such as vanishing points and road limits relatively easy, while the second one almost guarantees that objects in the scene will be well illuminated, simplifying obstacle detection and pattern recognition. The environments where we expect to have our system working require relaxing the above assumptions to a point where most existing algorithms would produce either incorrect results or no results at all.

There are far fewer works on road and lane detection in semi-structured environments. Along this line there are works based on techniques as diverse as template matching [5], neural networks [12], color-based region segmentation [1], morphological modelling and segmentation [4, 2], matched filters [8] and steerable filters [15]. Even though all these works are able to cope with poor road marking and other uncertainties in the environment, none of them works on videos acquired at nighttime. For instance, template matching and morphological approaches are not robust enough to handle images with very high levels of noise and lots of spurious features, and color-based segmentation is not appropriate because chromatic information is almost entirely lost under nighttime illumination. Moreover,

Proceedings of the XVII Brazilian Symposium on Computer Graphics and Image Processing (SIBGRAPI'04)
1530-1834/04 $ 20.00 IEEE

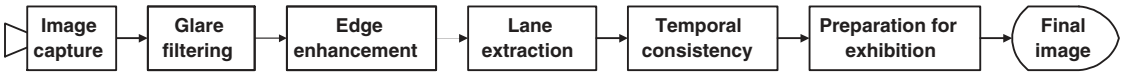

Figure 1. Functional diagram of the proposed Nighttime-Driving Assistance System.

all such works aim only at augmenting images with useful elements such as virtual road-marks, none of them removes from the images spurious elements that distract and confuse the drivers.

The system introduced in this paper, on the other hand, initially reduces or even cancels the effects of glare from light beams in the images, which not only eliminates a major distraction for human drivers, but facilitates subsequent steps of automatic road detection and tracking. Glare regions are identified as roughly circular areas with saturated pixel intensities in the input images, from which intensity values decay radially. Through a careful analysis of the rate of decay of average intensities along these radial lines, the additive contribution of glare to pixel intensities is estimated and then subtracted from the input images.

In addition, the proposed system uses robust techniques in order to detect and enhance the relevant road features such as lane-marks and road shoulders even in images with low signal-to-noise ratio. Under such conditions feature detectors tend to produce lots of false positives. In order to filter them out, our methodology exploits the facts that: (1) lanes and shoulders are usually parallel and thus they share common vanishing points that can be reliably and efficiently detected with a robust model-fitting algorithm known as RANSAC [6] and (2) this vanishing point typically moves little from frame to frame in continuous image streams, hence vanishing point positions estimated at previous frames can be used as a strong bias during the detection of features in the current frame.

Thus, the main contributions of this work are: (1) the development of an automatic and efficient (real-time) technique to reduce glare caused by light beams of other cars, which as far as we know is unique in the ITS literature, (2) the use of robust model-fitting and high-level knowledge about scene geometry to perform reliable and efficient (real-time) lane detection in the presence of high levels of noise, and (3) the exploration of the temporal continuity in the input image sequences, in order to guarantee that enhancements in the input images (such as the addition of virtual road-markers) are performed in a temporally-consistent way, *i.e.*, without high-frequency variations that are inconsistent with the scene's dynamics.

Next, in Section 2, a high-level description of the whole system is presented. In Sections 3 to 6, the major components of the algorithm are described. Implementation details are described in 7. Experiments with real video streams are presented and analyzed in Section 8, which is followed by our concluding remarks and considerations about future works (Section 9).

2. The Nighttime-Driving Assistance System

The proposed driving assistance system focuses on two tasks that must be accomplished in real time: (1) glare reduction and (2) enhancement of road surface and road and lane boundaries. A functional diagram of this system is depicted in Figure 1, where data flows from left to right.

In the first step, image capture from an external environment is accomplished with a video camera equipped with a CCD array that is sensitive not only in the visible spectrum, but also in the near-infrared. This broader sensitivity range increases the amount of information available to the system under subdued lighting conditions.

After it is captured, each frame goes through pre-processing steps whose goals are to filter glare effects out of the image and to enhance relevant road elements such as lane-marks to facilitate the posterior identification of the scene's geometry. Sections 3 and 4, respectively, provide detailed descriptions of these two tasks.

Each pre-processed image is then passed on to the lane extraction step where the road is identified and its major geometric elements (the lane-dividing lines and the road border) are extracted and the vanishing point is estimated. Due to high levels of image noise, these extracted features may be unstable from frame to frame. In order to eliminate this difficulty, positional consistency of the major scene elements is enforced across consecutive frames, in what we call a temporal consistency step. In sections 5 and 6, respectively, there are detailed descriptions of these two steps.

Finally, the results from all previous steps are combined in order to produce a final video stream, which is displayed to the driver in real time.

3. Glare filtering

The human visual system suffers considerable performance degradation under low levels of luminosity. Capabilities such as spatial resolution, contrast sensitivity and depth perception are diminished, while adaptation times for sharp luminosity variations increase [17, 18]. This degradation is one the main factors that lead to nighttime accidents [13, 11]. Glare caused by beams from incoming vehicles aggravates this perceptual problem because it forces immediate adaptation to steep variations of illumination in-

tensity. In the presence of glare, objects are often poorly defined, which hinders the identification of important navigation elements such as the road surface and various obstacles. This problem is especially serious when road-marks are faded due to improper maintenance and their radiometric properties become not very different from those of the surrounding environment.

In this work, glare-reduction efforts focus on the visual phenomena caused by intense lights usually originated from incoming vehicles. These lights cause saturation of the pixel intensities in certain image regions inside which all information about the scene is lost. We call the central, completely-saturated part of each image region affected by glare a *primary glare region*. In addition to this primary region, there is a circumscribing area that is appreciably affected by the effects of glare, but on which intensities are not completely saturated. This "diffusion" of glare across the image occurs due to the non-ideal focusing of the incoming car beams, the non-ideal optical properties of camera's lens and the bleeding of charge between neighboring CCD elements. The effects of glare on these non-saturated areas, which we call *secondary glare regions*, are stronger near the primary glare region and decrease radially.

The glare filtering algorithm starts with the identification of the primary glare regions. To simplify this task, the camera's shutter speed, optical aperture and channel gains are set in such a way that only direct light sources produce saturation in image intensities. With this configuration, primary glare regions can be identified simply thresholding the image at a near-saturation intensity level and then by detecting the contours of all connected components formed by the high-intensity pixels [20]. Each such connected component that meets a minimum area requirement gives rise to a primary glare region (Figure 2a). The boundary of this region is obtained by fitting an ellipse to the contour of its saturated connected component (Figure 2b), using the methodology suggested by Fitzgibbon and Fisher [7].

Based on this elliptical boundary, a *primary radius*, r, for the glare region is defined as shown in Figure 2c. The secondary glare regions are defined as a family of concentric circular rings such that the i-th secondary glare region is enclosed between circumferences of radii $i\,r$ and $(i+1)r$ (Figure 2d). The average intensities on all such regions are used to estimate how the influence of glare decays with the distance to the center of the primary glare region.

Beyond a pre-defined number of secondary glare regions it is assumed that the influence caused by glare is negligible. By intersecting all such "no-influence" areas relative to each glare region in the image, we identify all pixels that are not influenced by glare. The average intensity of these pixels, which we call *average background intensity*, when subtracted from the average intensity of each secondary glare region, provides an estimate of the additive in-

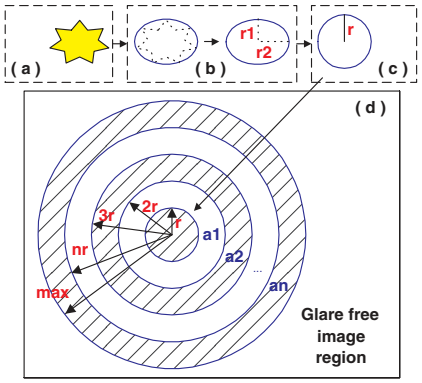

Figure 2. Labelling of glare regions. (a) Detection of a connected component of saturated pixels; (b) Computation of the *primary glare region*; (c) Computation of the *primary radius*, $r = (r1+r2)/2$; (d) Definition of the *secondary glare regions*.

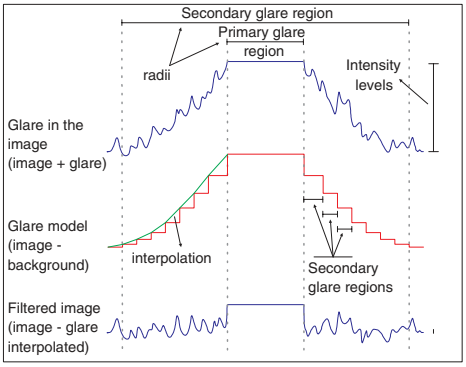

Figure 3. Glare modelling and filtering. By averaging intensity values within each *secondary glare region* and subtracting the *average background color*, a stairway-like model of radial glare decay is obtained. Linear interpolation eliminates discontinuities. Subtraction of the resulting model from input intensities filters glare out.

fluence of glare on the image.[1] In order to eliminate discontinuities in this estimate at the circular boundaries between secondary glare regions, its values are linearly interpolated along the radial direction (Figure 3). Finally, by subtracting the glare estimates from the input images we obtain images

1 Even though pixels in the primary glare region are also affected by glare, their information content is almost zero due to saturation. Thus, it is impossible to enhance the image at those points unless auxiliary sensors (*e.g.* a second camera with neutral density filters) are used.

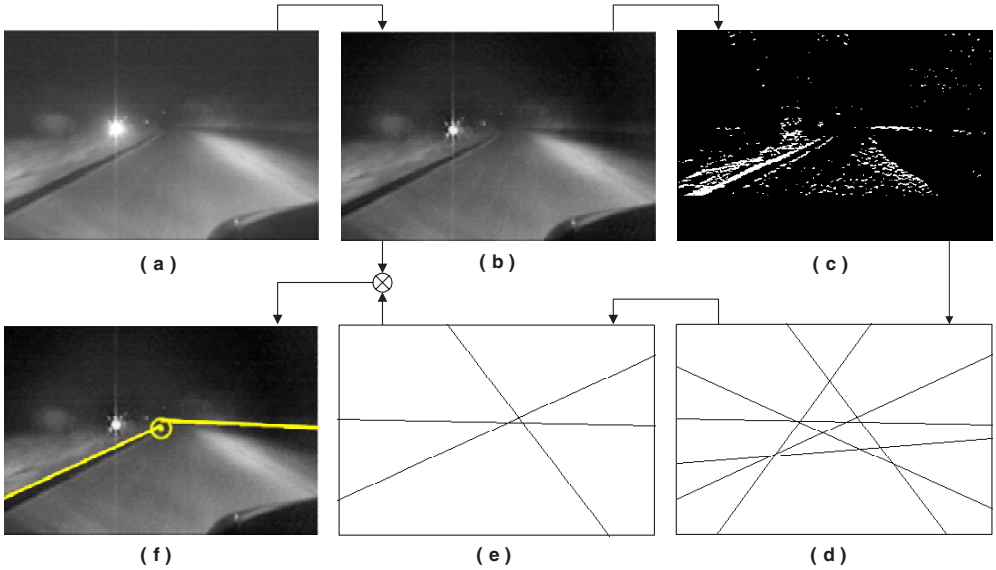

Figure 4. Major steps in the complete processing of a real input image. (a) Raw input image; (b) Glare reduction; (c) Edge detection; (d) Extraction of consistent straight line segments; (e) Vanishing point calculation and elimination of outliers (f) Enforcement of temporal consistency and assemblage of the output image for exhibition.

where the effects of glare are cancelled everywhere but in the primary glare regions. The result of applying this technique to a real image is shown in Figure 4 (a and b).

A performance-optimized version of the *Basic Glare Filtering Algorithm* described above was also implemented. The *Optimized Glare Filtering Algorithm* uses a training set of real images affected by glare to compute *a priori* models of radial glare decay. For each integral value of the primary radius (r) found in this training set, a unique *a priori* model of glare decay is computed by averaging the individual radial decay models of all r-radius glare instances. After this initial training phase, when a glare instance is found in the live input stream, all that is needed is to compute its primary radius and then to apply the proper decay model for that radius. No glare modelling needs to be done in real time. Experiments performed on real data (Section 8) indicate that the Optimized Algorithm is significantly faster but less accurate than its Basic counterpart.

4. Edge detection

Edge detection is a technically trivial but nonetheless necessary step in our methodology. Its goal is to identify image features that elicit the scene's important geometric elements such as lane-dividing lines and road borders.

In this work, edge detection starts with the application to each input image of a standard high-pass filter (such as Prewitt) that outputs a value proportional to the magnitude of a spatial image gradient at each pixel. The caveat is that if the identification of the *edgels* (*i.e.* the pixels that belong to some edge) is performed with a simple threshold of the resulting gradient image, then either a few relevant but faded lines are not detected (if the threshold is set high) or too many isolated, useless edgels are selected (if the threshold is set low). In order to keep the edgels that belong to faded lines and eliminate those that are isolated, we apply a low-pass filter to the gradient image and then select any pixel as an edgel if and only if its intensities in both the image output by the high-pass filter and the one output by the low-pass filter exceed pre-defined thresholds. The result of this operation on real data is shown in Figure 4 (b and c).

5. Road-mark extraction

The goal in this step is to identify the major task-relevant scene elements such as road-marks in a way that is geometrically and temporally consistent. Due to the low signal-to-noise ratio of the input images acquired under nighttime illumination, this is a difficult task. As shown in Figure 4c, a large fraction of edgels selected at the end of the edge detection step are outliers, *i.e.* data that do not belong to any of the elements that we want to extract. In order to make the system work reliably is this scenario we make use of two powerful ideas:

To exploit the temporal consistency of the input stream: Because cars are vehicles with non-holonomic dynamics, their orientation relative to the scene typically varies smoothly. Hence the positions of important scene elements such as vanishing points typically change little from frame to frame in a live, 30 frames-per-second input stream. This means that knowledge of such positions at frame $t-1$ can be used as a strong bias on the location of the relevant scene elements at time t.

To enforce the global geometric consistency of the scene: The fact that all road-marks of any given straight road segment form a line pencil (*i.e.* they meet at a single vanishing point in each image) is a powerful constraint that can be used to separate inliers from outliers efficiently and reliably. Planar line pencils are very simple geometric structures that can be identified easily by robust model-fitting algorithms.

The first step in our road-mark detection methodology is the identification of visible straight line segments that are consistent with $\hat{\mathbf{v}}_{t-1}$, the vanishing point found for the last frame of the input stream.[2] This is done through a modified Hough transform [21] in which only lines whose distance to $\hat{\mathbf{v}}_{t-1}$ does not exceed a pre-defined threshold, $d_{\max}$, are included in the voting space. The standard Hough transform has been used by other authors for road-mark detection (albeit in structured environments) [14, 19], but the modification described above is essential to make it efficient enough for execution at frame rate.

In addition, to improve the geometric consistency of the results, votes for lines that are closer to $\hat{\mathbf{v}}_{t-1}$ are weighted more than votes for lines that are further away from it, and votes coming from edgels that have neighbors along the direction of the lines they are voting for are weighted more than those coming from isolated edgels. More specifically, each edgel $\mathbf{e}$ casts a vote for each line $\mathbf{l}$ in the Hough space that contains $\mathbf{e}$ and has a distance to $\hat{\mathbf{v}}_{t-1}$ not larger than $d_{\max}$. But each such vote is weighted according to a weight

$$w(\mathbf{e},\mathbf{l}) = \frac{d_{\max} - \mathrm{dist}\,(\mathbf{l},\hat{\mathbf{v}}_{t-1})}{d_{\max}} + \frac{L\,(\mathbf{e})}{L_{\max}}, \qquad (1)$$

where the function dist measures the Euclidean distance between a line and a point, $L(\mathbf{e})$ is the length of the longest continuous linear chain of edgels along the direction of $\mathbf{l}$ that ends in $\mathbf{e}$, and $L_{\max}$ is a pre-defined upper bound on L (if $L\,(\mathbf{e})$ exceeds $L_{\max}$ then it is set to $L_{\max}$). The result of this modified Hough transform on real data is shown in Figure 4 (c and d).

2 Here and in the rest of this paper, we assume that the entire road section visible is straight. Road sections that are not straight can be handled by modifying the methodology described so that multiple vanishing points are estimated at each frame, rather than just one.

It can be observed that, even though the lines selected have some degree of geometrical consistency, they do not meet exactly at a single point. This happens not only due to the effects of image noise, but especially because the actual position of the vanishing point typically varies by an amount that is small but not negligible between consecutive frames of the input stream. Thus, $d_{\max}$ must be set to values that are not small enough to prevent the existence of a few outliers in set of straight lines selected by the Hough transform. In order to be able to prune these outliers out and then to estimate the current vanishing point position with high precision, we use a robust model-fitting technique known as RANSAC [6].

The key idea behind RANSAC is to select, at random, subsets of the available data that contain the *minimum* amount of information necessary to estimate all parameters in a given model. In the identification of a line pencil, for instance, each such minimal data subset consists of two lines, because two distinct lines are necessary and sufficient to define a unique intersection point.[3] Once the model is instantiated (*i.e.* the coordinates of the vanishing point are calculated) based on a minimal data subset, all other data (lines) that are consistent with the model instance produced (*i.e.* those whose distance to the calculated vanishing point is smaller than a predefined consistency threshold, $\delta_{\max}$, typically much smaller than the Hough transform's threshold $d_{\max}$) are found. After N_{iter} minimal data subsets are independently chosen, the model instance that is consistent with the largest subset of the available data is selected.

RANSAC is a probabilistic algorithm. Its output may vary across different executions, but it finds parametric models on data contaminated by large proportions of outliers with an arbitrarily high success probability, P_{succ}, if the number of iterations of its main loop is set as

$$N_{\mathrm{iter}} = \left\lceil \frac{\log\left(1 - P_{\mathrm{succ}}\right)}{\log\left(1 - {R_{in}}^{m}\right)} \right\rceil, \qquad (2)$$

where R_{in} is the ratio of inliers to total data and m is the number of elements in each minimal data set. In our application R_{in} is so large and m is so small that we can choose P_{succ} very close to one without a negative impact on the system's performance. The effects of RANSAC on real data can be observed in Figure 4 (d and e).

6. Temporal consistency

In our road-mark detection methodology, the position estimation of the vanishing point at frame $t-1$ strongly constrains the set of possible locations where this point may

3 Two parallel lines meet at a point at infinity. This corresponds to a singularity if points and lines are represented in Euclidean coordinates, but not if they are represented in projective coordinates.

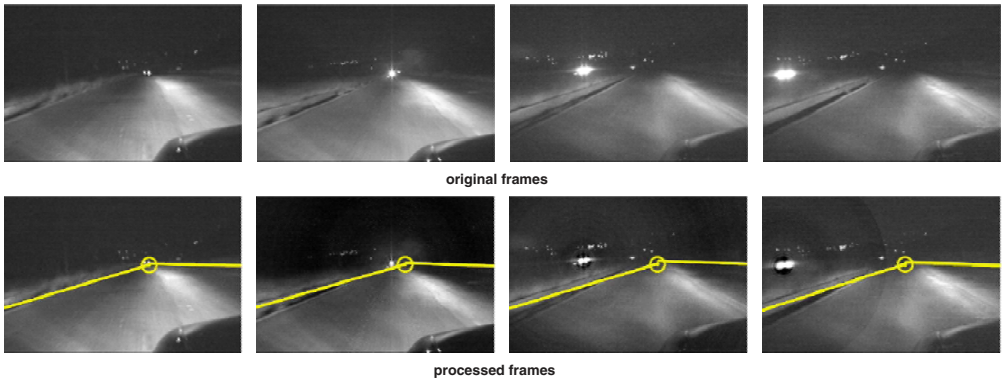

Figure 5. Sequence of frames enhanced in a temporally-consistent way. The top row corresponds to input frames taken from a live 30 f.p.s. video stream. The bottom row corresponds to the respective enhanced images output by the system.

be found at frame t. Nonetheless, there are no hard constraints which link individual road-marks at frame t to those at frame $t-1$. Because of this, and as a result of image noise and unpredictable fluctuations both in illumination and in the reflectance characteristics of scene elements, positions estimated for individual road-marks may suffer unnatural high-frequency variations. Also, road-marks that are correctly detected on a given frame may suddenly "disappear" in the next frame.

Blinking and shifting road-marks, even if located close to their ideal image positions will definitely distract and annoy the driver instead of providing assistance. Therefore, in order to provide a consistent and smooth display of the results generated by our methodology, a time-averaging scheme is used to create stable virtual road-marks from the time-varying sets of inliers output by RANSAC.

A data structure which we call Road-Mark Buffer is used to store the "history" of each virtual road-mark. Each virtual road-mark stored thereof has a scalar field called *consistency*, which measures how frequently it has come up in the data in the last few frames. At each new frame processed, all inliers output by RANSAC are matched against the existing virtual road-marks. Those inliers that do not match any existing virtual road-mark become a virtual road-mark on their own, whose consistency is initially set to a low value. The other ones are added to the records of their respective matches, whose consistencies are incremented at each "hit", up to a pre-defined maximum value. On the other hand, every time a virtual road-mark is not found in a frame, its consistency is decremented and it becomes zero, the road-mark's record is deleted from the Road-Mark Buffer.

Only the virtual road-marks whose consistency is above a threshold are actually displayed and their intensity in the output stream is set proportional to their consistency. Moreover, to further stabilize the output stream, the position and orientation on which each virtual road-mark is exhibited are calculated from weighted averages of the parameters of all lines in the road-mark record. Such weights are initially set proportional to the score of each line on the modified Hough transform described in Section 5. The weights decay exponentially at each iteration. To save space, a maximum number of K lines per virtual road-mark record is established and only the K lines with largest weight are kept when the processing of each frame is finished. The temporal consistency in the output stream generated by this scheme can be observed in Figure 5.

7. Implementation

Three main libraries where used during the system's implementation. Microsoft's *DirectX* , a high-performance library designed for implementation of games and multimedia applications, was used to code the video capture module, as well as the structural part of the frame processing module. *IPL* (Image Processing Library) and *OpenCV* (Open Source Computer Vision Library), which are libraries designed for high-performance image processing and computer vision, respectively, were used to implement the rest of the frame-processing module. To use and integrate these technologies and code the rest of the system the C++ and COM programming languages where used.

8. Results

This section presents the results obtained by the system with real images acquired at a typical Brazilian road, at night, with a SONY camera equipped with a zoom lens (4.2–42 mm), and with the near infra-red option turned on. The computer was a Pentium III with two 450 MHz processors, 512 of RAM and running the Windows 2000 Profes-

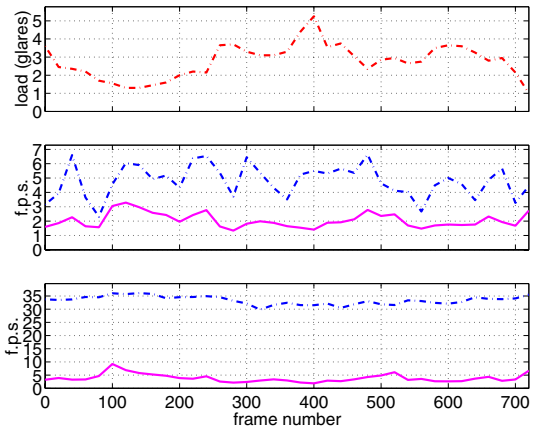

Figure 6. Performance of the developed system on continuous, 30 frames-per-second (f.p.s.) input video streams. Top: the number of processed glares per frame is used as a measure of system load. Middle, bottom: frames per second achieved on the output stream, respectively, when both glare reduction and virtual road-mark overlay are performed, and when only glare reduction is performed. The solid (magenta) and dash-dotted (blue) lines refer, respectively, to the *Basic* and *Optimized Glare Filtering Algorithms*, described in Section 3.

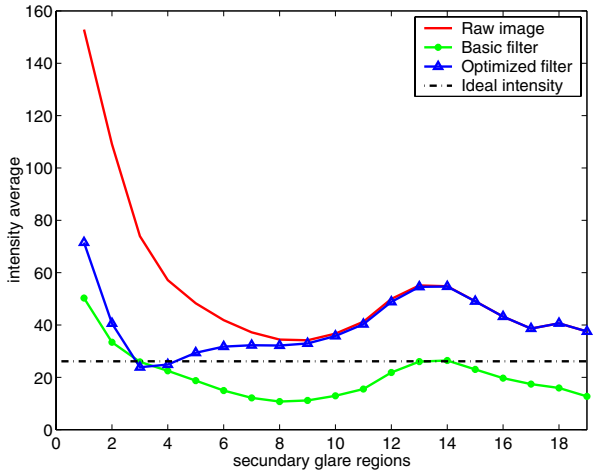

Figure 7. Average pixel intensities as a function of the distance to the center of the closest *primary glare region*. The three solid lines refer to the averages obtained in the raw images (without glare filtering) and after the application of the *Basic* and *Optimized Glare Filtering Algorithms* (see legend). The dash-dotted (black) line is the ideal intensity value after the subtraction of glare, obtained from the pixels that are outside all glare areas.

sional operating system. The experiments where designed to validate and evaluate the performance and precision of both the glare reduction techniques and the lane-mark detection methods.

The first experiment (shown in Figure 6) estimated the frame rate obtained by the system using the two proposed glare reduction techniques, both with and without lane-mark detection activated. The number of processed glares per frame is used as a measure of system load. Approximately 30 seconds of video were acquired using only the frames that contained glares (715 out of a total of approximately 900 frames). The graph shows that performance of both glare-reduction techniques is roughly inversely proportional to the number of glares detected. Another important fact is the significant performance improvement of the Optimized Glare Filtering Algorithm with respect to the Basic one, achieving rates 1.5 to 3 times larger with lane-mark detection activated, and 4 to 15 larger times with it deactivated.

The second experiment (presented in Figure 7) compared the quality of both glare reduction techniques. Data from the same 30 s stream used in the first experiment were used. It can be observed that the Basic Glare Filtering Algorithm

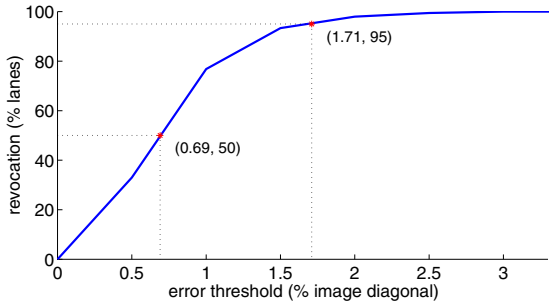

Figure 8. Precision of the virtual lane-marks.

obtained results that are closer to the ideal ones than the Optimized version. But still both techniques improve the quality of the images significantly with respect to the raw video stream.

The objective of the last experiment (Figure 8) was to evaluate the quality of the results obtained by the lane-mark detection module. The experiment was performed on 500 frames of continuous video (approximately 18 seconds) in which reference lane-marks marked manually and lane-marks automatically detected by the system were compared.

The area between each reference lane-mark and the detected lane-mark, divided by the length of the projection of the detected lane-mark on the reference lane-mark was used as an error metric. Each one of these values was then compared to the image diagonal and their ratio was computed. With these data, a revocation graph was plotted where the X-axis represents the error relative to the length of the image diagonal, and the Y-axis represents the percentage of lane-marks that have an error bellow each given threshold in the X-axis. Based on the presented data, our lane-mark detection system performed well, with errors below 2% of the diagonal length for 95% of all lane-marks processed.

9. Conclusion

This paper described a system to assist drivers in semi-structured environments under low illumination by providing significant reduction in the amount of glare caused by oncoming traffic and by generating "virtual" lane-marks. Two glare reduction methodologies were developed and tested with real data. Both techniques were found to be adequate for frame-rate applications. Moreover, a robust methodology for lane detection was designed and implemented. It is based on accurate determination of the vanishing point for the road and temporally-consistent estimation of line pencils in the image plane.

In spite of the fact that the developed system had a reliable behavior in several tests conducted with real data, there is still a long way to go before it can be deployed on real vehicles. Sharp turns and occlusion caused by roadside obstacles are some examples of difficult, albeit frequent problems such a system may face under normal operation. Further work is needed in order to deal with these difficulties. Other potential improvements include the user interface, which should be as transparent as possible to the user. This might involve devices such as liquid-crystal screens adapted to windshields. Finally, but very importantly, psychophysical experiments need to be performed in order to evaluate the actual gain for the human user.

Acknowledgements

This research has been supported by CNPq, by Fapemig and by PRPq-UFMG (Fundo Fundep RD).

References

[1] S. L. M. Beuvais and C. Kreucher. Building world model for mobile platforms using heterogeneous sensors fusion and temporal analysis. In *Proc. IEEE Intl. Conf. Intelligent Transportation Systems*, page 101, 1997.

[2] A. Broggi. Robust real-time lane and road detection in critical shadow conditions. In *Proc. IEEE Intl. Symp. Computer Vision*, pages 353–358, 1995.

[3] A. Broggi, M. Bertozzi, A. Fascioli, and G. Conte. Vision-based intelligent vehicles: state of the art and perspectives. *Robotics and Autonomous Systems*, 32:1–16, 2000.

[4] A. Broggi, G. Conte, F. Gregoretti, C. Sansoè, and L. M. Reyneri. The evolution of the paprica system. *Integrated Computer-Aided Engineering J.*, 4(2):114–136, 1997.

[5] C. J. D. and T. C. E. Unscarf: a color vision system for the detection of unstructured roads. In *Proc. IEEE Int. Conf. Robotics and Automation*, pages 2496–2501, 1991.

[6] M. A. Fischler and R. C. Bollesm. Random sample consensus: a paradigm for model fitting with applications to image analysis and automated cartography. *Comm. ACM*, 24(6):381–395, 1981.

[7] A. W. Fitzgibbon and R. B. Fisher. A buyer's guide to conic fitting. In *Proc. British Machine Vision Conf.*, pages 513–522, 1995.

[8] S. Gehrig, A. Gern, S. Heinrich, and B. Woltermann. Lane recognition on poorly structured roads - the bot dot problem in california. In *Proc. IEEE Intl. Conf. Intelligent Transportation Systems*, 2002.

[9] M. Green and J. W. Senders. Human error in road accidents. *Swiss Reinsurance Canada Review*, 6(9):1–14, 2000.

[10] U. Handman, T. Kalinke, C. Tzomakas, M. Werner, and W. Seelen. An image processing system for driver assistance. In *Proc. IEEE Intl. Conf. Intelligent Vehicles*, volume 2, pages 481–486, 1998.

[11] R. D. Hazlett and M. Allen. The ability to see a pedestrian at night : The effects of clothing, reflectorization and driver intoxication. *Am. J. Optometry*, 45(4):246–258, 1968.

[12] K. I. Kim, S. Y. Oh, S. W. Kim, H. Jeong, C. N. Lee, B. S. Kim, and C. S. Kim. An autonomous land vehicle prv ii: Progresses and performance enhancement. In *Proc. IEEE Intelligent Vehicles Symp.*, pages 264–269, 1995.

[13] H. W. Leibowitz and D. A. Owens. We drive by night. *Psychology Today*, 20(1):55–58, 1986.

[14] J. B. Mc Donald, J. Franz, and R. Shorten. Application of the hough transform to lane detection in motorway driving scenarios. In *Proc. Irish Signals and Systems Conf.*, 2001.

[15] J. C. McCall and M. M. Trivedi. An integrated, robust approach to lane marking detection and lane tracking. In *Proc. IEEE Intelligent Vehicles Symp.*, 2004.

[16] D. Owens and M. Sivak. Differentiation of visibility and alcohol as contributors to twilight road fatalities. *Human Factors*, 38(4):680–689, 1996.

[17] S. Plainis, K. Chauhan, I. J. Murray, and W. N. Charman. Retinal adaptation under night-time driving conditions. In *Proc. Vision in Vehicles VII*, 1997.

[18] S. Plainis, I. J. Murray, K. Chauhan, and W. N. Charman. Reaction times as an index of visual conspicuity at night. In *Proc. Vision in Vehicles VIII*, 1999.

[19] K. Sobottka and H. Bunke. Detection of road boundaries in range image sequences. In *Proc. Intl. Symp. Automotive Technology and Automation*, pages 129–136, 1999.

[20] S. Suzuki and A. K. Topological structural analysis of digital binary images by border following. *Computer Vision, Graphics, and Image Processing*, 30(1):32–46, 1985.

[21] E. Trucco and A. Verri. *Introductory Techniques for 3-D Computer Vision*. Prentice Hall, 1998.